WATER RESOURCES RESEARCH, VOL. 33, NO. 4, PAGES 611–623, APRIL 1997

Soil water depletion by oak trees and the influence of root water uptake on the moisture content spatial statistics

Gabriel Katul, Philip Todd, and Diane Pataki
School of the Environment, Duke University, Durham, North Carolina

Zbigniew J. Kabala
Civil and Environmental Engineering, Duke University, Durham, North Carolina

Ram Oren[1]
School of Environment, Duke University, Durham, North Carolina

Abstract. The space-time statistical structure of soil water uptake by oak trees was investigated in a 3.1-m-diameter closed top chamber using a three-dimensional measurement grid of soil moisture and pressure, and measurements of tree transpiration. Using the time domain reflectometery (TDR) measured moisture content, resistance block measured soil water pressure, and a compact constant head permeameter measured saturated hydraulic conductivity, the soil hydraulic properties for the chamber were first estimated. Then, dimensionless statistical measures that utilize the soil water pressure were proposed and used to assess the relative importance of lateral to vertical flow. On the basis of the measured statistical properties of the soil-water pressure, it was found that the vertical flow is at least an order of magnitude larger than the lateral flow, and thus a one-dimensional flow approximation to continuity was utilized. Using continuity and a first-order Taylor series expansion of the Buckingham-Darcy vertical flux about the spatial mean moisture content state, an approximate relation for the time variation of the spatial mean moisture content was derived and tested with the TDR measurements. Despite a large spatial coefficient of variation in the TDR measured moisture content (which was also shown to be comparable to reported values from larger-scale field experiments), good agreement between mean moisture content predictions and measurements were found for two separate drying cycles. The approximate Taylor series flux expansion was utilized for deriving an analogous relation for the time variation of the spatial moisture content variance. The resultant variance budget was used to assess the role of root water uptake on the spatial variability of moisture content. It was found that the root uptake component, which resulted from a covariance between the root water uptake and moisture content spatial perturbations, is comparable to the contribution from soil hydraulic properties and soil water redistribution. One of the main findings in this study is that root water uptake is central to the moisture content spatial variance dissipation especially for dry soil moisture conditions. These results were further investigated using Monte-Carlo simulations.

1. Introduction

Mathematical description of water flow in the unsaturated zone near the land-atmosphere interface is complicated by uncertainties in the description of the soil hydraulic properties and has been the subject of active research for the past 2 decades following the study by *Nielsen et al.* [1973]. An additional complication that arises in this near surfacial zone is the active role of root water uptake. In practice, one of the assumptions made in the field description of spatial variability in moisture content is the neglection of this variability relative to the variability imposed by the soil hydraulic properties [see, e.g., *White*, 1988; *Clapp et al.*, 1983]. Justification for this approximation rests on the observation that transpiration does not vary appreciably in the field when compared to the soil hydraulic properties. Currently, our ability to separate the spatial variability in moisture content due to root water uptake from variability in soil hydraulic properties is not well developed. *Clothier* [1988] suggested that all important small-scale heterogeneity in the near-surface moisture content can be engendered by root water uptake, especially in forested watersheds.

This study considers the influence of root water uptake on the spatial statistics of soil moisture content close to the land-atmosphere interface. For this purpose, a prognostic equation for the moisture content spatial variance budget is developed in order to set a framework for explicitly quantifying the relative contribution of root water uptake on the moisture content spatial variance. Then a controlled experiment was carried out in a closed-top chamber, 3.1 m in diameter, planted with

[1]Also at Jet Propulsion Laboratory, Science Division, Pasadena, California.

Paper number 96WR03978.
0043-1397/97/96WR-03978$09.00

3-year-old oak trees (*Quercus phellos L.*), and equipped with a three dimensional measurement grid of soil water content and pressure, and sap flow gauges at the base of one seedling to investigate the soil water budget for such idealized conditions. The spatial scale of the chamber is much larger than the "laboratory" scale, but much smaller than the field scale which is ideal for partitioning variability between root water uptake and soil hydraulic properties. The specific objectives are to assess the role of root uptake on the time variation of (1) the spatial moisture content mean; (2) the spatial moisture content variance; and (3) the transpiration and its relation to the soil water redistribution in the root zone.

2. Theory

The one-dimensional soil water transport continuity equation with root water uptake is given by

$$\frac{\partial \theta}{\partial t} = -\left(\frac{\partial q}{\partial z} + S\right) \tag{1}$$

where θ is the volumetric soil moisture content, q is the vertical flux, t and z (directed positively downward) are the time and depth, respectively, and S is the water uptake by the roots at depth z [e.g., *Warrick*, 1974; *Markar and Mein*, 1987]. The one-dimensional flow approximation is valid if the vertical pressure gradients are much larger than the horizontal pressure gradients, and the root uptake variability in the vertical is much larger than the variability in the lateral direction, respectively. The later is valid for trees due to the strong vertical variability in the root density per unit depth (ρ_r). In this study, the term "much larger than" applies when one variable is at least an order of magnitude larger than another variable. Within the chamber, spatial variability of soil hydraulic properties and root uptake are not negligible and the statistical approach is utilized.

2.1. Time Variation of the Volume-Averaged Moisture Content

Consider the cylinderic local volume averaging operator $\langle\square\rangle$ over chamber area A and TDR rod length L_R such that the volume averaging of a variable u is

$$\int_A dA \int_{L_R} u\, dz = \langle u \rangle \tag{2}$$

where $A(=\pi R^2)$, $R(=1.5$ m) is the chamber radius, and L_R is set at 0.1 m in this study. This averaging is necessary in order to match the scale of the theory to the vertical scale of the TDR measurements. By applying this volume averaging operator to (1), the time variation of the volume-averaged moisture content within the chamber for a layer thickness L_R is given by

$$\frac{\partial \langle \theta \rangle}{\partial t} = -\left(\frac{\partial \langle q \rangle}{\partial z} + \langle S \rangle\right) \tag{3}$$

Notice in (3) that $\langle q \rangle$ and $\langle S \rangle$ are necessary to the description of $\langle \theta \rangle$. To estimate $\langle q \rangle$, consider the Buckingham-Darcy isothermal flux approximation

$$q = -K(\theta)\frac{dH}{dz} \tag{4}$$

where $K(\theta)$ and $H(\theta)$ $(=\Psi(\theta) - z)$ are the soil hydraulic conductivity function and soil matric potential, respectively, and $\Psi(\theta)$ is the soil water suction. The root water uptake, as a function of θ, is not known, but conservation of liquid mass for the tree system requires that

$$T = \int_0^h \langle S(z) \rangle\, dz \tag{5}$$

where h is the root-zone depth and T is the total water flux at the base of the tree stems within the chamber. In (5), the liquid water storage per unit time within the root system is neglected relative to the amount transported through the tree stem. Volume averaging (4) and (5) is necessary to the solution of (3), but this cannot be achieved analytically since q is a nonlinear function of θ and a closure problem arises [see, e.g., *Katul et al.*, 1993; *Parlange et al.*, 1993; *Wendroth et al.*, 1993]. In the following section, an approximate approach that is based on a linearized Taylor series expansion for the flux is considered.

To evaluate $\langle q \rangle$, the approximation

$$\langle q \rangle = -\left\langle K(\theta)\frac{dH}{dz}\right\rangle \approx -K(\langle\theta\rangle)\frac{dH(\langle\theta\rangle)}{dz} \tag{6}$$

is used and is derived from a Taylor series expansion of q around $\langle\theta\rangle$, neglecting all but the first two terms, and applying the volume averaging operator. Further discussion on (6) can be found in Appendix A. For a nonhysteretic soil redistribution process and for the range of θ encountered in this experiment, $K(\theta)$ and $\Psi(\theta)$ can be described by the *Clapp and Hornberger* [1978] relations

$$K(\theta) = K_s\left(\frac{\theta}{\theta_s}\right)^{2b+3} \tag{7}$$

$$\Psi(\theta) = \Psi_s\left(\frac{\theta}{\theta_s}\right)^{-b} \tag{8}$$

where K_s and Ψ_s are the near-saturated hydraulic conductivity and soil-water tension, θ_s is the near-saturated moisture content, and b is an empirical parameter that varies with soil texture [see also *Campbell*, 1974; *Brooks and Corey*, 1964]. In essence, this approximation replaces the nonuniform soil water redistribution–plant water uptake system by an equivalent uniform soil-plant system such that the state variable of this system (θ) is identical to $\langle\theta\rangle$. Hence, given the soil hydraulic properties and the root water uptake, the time variation of $\langle\theta\rangle$ can be computed using (3)–(5). The numerical schemes, boundary conditions, and suggested approximations to (5) are discussed in Appendix B.

2.2. Time Variation of the Volume-Averaged Soil Moisture Content Variance

The time variation of the spatial soil moisture content variance $\langle\theta'^2\rangle$ (hereafter referred to as variance budget) around $\langle\theta\rangle$ can be determined by subtracting (3) from (1), multiplying the result by θ' and volume averaging to give

$$\frac{\partial \langle \theta'^2 \rangle}{\partial t} = -\left(2\left\langle \theta' \frac{\partial q'}{\partial z}\right\rangle + 2\langle \theta' S' \rangle\right) = -(P_I + P_{II}) \tag{9}$$

where $\theta' = \theta - \langle\theta\rangle$, $q' = q - \langle q\rangle$ and $S' = S - \langle S\rangle$ (see Appendix A for assumption details). Notice that in the absence of any matric potential gradients and root uptake, (9) becomes $\partial\langle\theta'^2\rangle/\partial t = 0$, and the solution to (9) reduces to $\langle\theta'^2\rangle = \text{const}$. For this ideal case, the constant can be determined from the initial conditions. For soil-plant systems, (9) implies that the time evolution of $\langle\theta'^2\rangle$ is governed by two redistribution pro-

cesses: (1) the interaction between the moisture content and flux-gradient spatial fluctuations (P_I) and (2) the interaction between moisture content and root-uptake fluctuations (P_{II}).

Whether these two processes produce or dissipate the spatial variability in moisture content can be conceptually considered using an idealized uniform soil with an initial soil moisture variability produced by nonuniformity in an applied water event (and/or infiltration capacity). In the absence of any external forces (e.g., gravity), soil water redistribution occurs in the direction of decreasing potential energy and water will flow from wetter to drier spots. In this study, the term redistribution refers to the continued water movement within a soil profile following an applied water event at the soil-atmosphere interface. At time $t = \infty$ it is expected that the soil moisture content will become evenly distributed and $\langle \theta'^2 \rangle \rightarrow 0$. Similarly, for a planar homogeneous root density profile, root soil water uptake will be large for wetter spots and small for drier spots; hence wetter spots will become drier at a faster rate when compared to drier spots. Both P_I and P_{II} tend to reduce the spatial variability in moisture content for a drying cycle and both processes are, to a first approximation, variance dissipation terms for uniform soils and root density profiles. The opposite may be true for term P_{II} in the presence of large variability in root density profiles.

For nonuniform soils and variable root response to environmental perturbations, the role of P_I and P_{II} on the variance budget in (9) is far from well understood, especially the covariance described by P_{II}. This, in part, is due to the lack of (1) direct measurements of S', (2) a complete theory that describes root soil water uptake as a function of θ (see, e.g., the magnetic resonance images of water depletion around roots by *Macfall et al.* [1990]), and (3) the rapid time variation in environmental parameters controlling T and S.

3. Experimental Setup

3.1. Study Site

The study site is situated within the Duke Forest, Durham, North Carolina (35° 52′ 00″ N, 79° 59′ 45″ W) in a transition zone between the Coastal Plain and the Piedmont plateau. The soil at the site was classified as an Appling sandy loam of the Helena series. The average elevation of the site is 130 m above mean sea level. Mean annual air temperature and precipitation for this region are 15.5°C and 1140 mm, respectively.

The site is used in collaboration with the U.S. Environmental Protection Agency (EPA) to investigate biogenic volatile organic compound (BVOC) emissions from trees in the southeastern United States. Nine experimental plots with closed growth chambers were used so that the atmospheric elements and BVOC concentrations can be accurately measured. The chambers are 3.1 m in diameter, 4.5 m in height, and protrude 8 cm into the soil at the base. The species considered are *Pinus taeda* L., *Liquidambar styraciflua* L., and *Q. phellos L.*, with each of the nine chambers planted uniformly by one of the above species. There were 32 three-year-old saplings (height is 1.5 m) in each chamber planted at a 60 cm × 60 cm spacing. The edge trees were removed so that the chamber boundary will not affect growth during the experiment.

3.2. Measurement Grid in the Chamber

One of the oak chambers (chamber 56) was chosen for intensive soil moisture and pressure measurements. Fifteen measurement points were placed in a radial pattern as shown in Figure 1. Of these 15 points, two were outside the chamber in order to assess horizontal soil moisture movement across the chamber periphery.

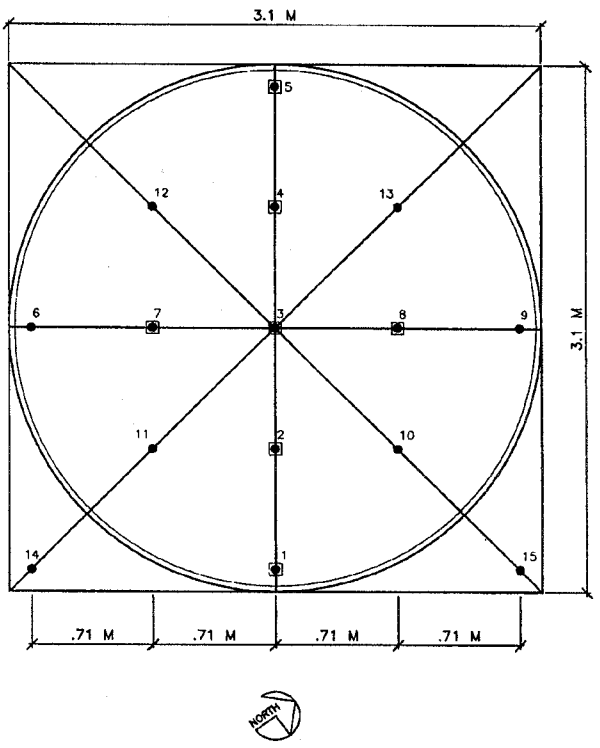

Figure 1. Time domain reflectometry (TDR) and resistance blocks measurements within and outside chamber 56.

3.2.1. Soil moisture content measurements. At each of the 15 measurement points, 3 pairs of stainless steel rods were installed at 0–10 cm, 0–20 cm, and 0–30 cm for time domain reflectometry (TDR) soil moisture content measurements. The TDR system is comprised of a cable tester (Tecktronics, Redmond, Oregon) which transmits an electromagnetic wave along stainless steel rods and then measures the propagation velocity (V_p). The resulting velocity is related to the relative dielectric constant of the soil κ using

$$\kappa = (LV_p/L_R)^2 \tag{10}$$

where L is the distance (cm) that the electromagnetic wave travels along L_R, and L_R is the rod length (m). The dielectric constant is highly sensitive to volumetric water content and weakly sensitive to soil types [*Cassel et al.*, 1994]. The dielectric constant of pure water is 80, while that of air is 1. Minerals fall at different values in between these two limits (e.g., 3–6) depending on their composition. To obtain θ from κ, the *Topp et al.* [1980] calibration curve, given by

$$\theta = -0.053 + 0.0292\kappa - 0.00055\kappa^2 + 0.0000043\kappa^3 \tag{11}$$

is used. This equation was validated for soils with low clay content [see *Topp et al.*, 1980; *Topp and Davis*, 1985; *Malicki and Skierucha*, 1989; *Gardner et al.*, 1990; *Roth et al.*, 1992] but proved to be less accurate for soils with high montmorillonite clay content [*Dasberg and Hopmans*, 1992], organic soils [*Herkelrath et al.*, 1991], and fine-textured soils [*Dasberg and Hopmans*, 1992].

The soils in the chamber have minimal clay content in the upper horizons, and (11) was used for calculating soil water content.

3.2.2. Soil water tension, total transpiration, and other environmental variables. At 9 out of the 15 points, resistance blocks (Watermark, Irrometer Co., Inc., Riverside, California) were installed at the same three levels as the TDR to monitor $\Psi(\theta)$. The Watermark sensor consists of two concentric electrodes buried in a reference matrix material that is held in place by a synthetic membrane. The matrix material has been selected to reflect the maximum change in electrical resistance over the growth range of production crops as well as to neutralize the effects of soil salinity. Soil moisture is constantly being absorbed or released from the sensor depending on the pressure balance between the block and the adjacent soil. As the soil dries out, the soil pressure around the sensor decreases and the sensor moisture is reduced due to flow of water from the block into the soil. This water loss is sensed by an increase in the electrical resistance between the electrodes. A thermocouple was installed near the center of the plot at 15 cm depth to measure soil temperature and was also used to correct the Watermark block resistance readings. According to a study by *Armstrong et al.* [1985], the Watermark blocks can accurately estimate soil water pressure for $|\Psi| < 2$ bars. These 27 blocks were connected to a Campbell Scientific 21x micrologger, sampled every 1 min, and averaged every 30 min. During the experiment, instantaneous volumetric soil water content, soil water potential, and soil temperature were each collected at least twice a day and up to four times a day during intensive measurement periods.

In the chamber, several environmental and physiological data were also collected on a 30 min time step though out the experiment. Air temperature was measured at 1 and 3 m above the ground surface, relative humidity and photosynthetically active radiation (PAR) were also measured at the same time increment.

To estimate T, a representative seedling was equipped with three sap flux gauges (Dynagage, Dynamax, Inc., Houston, Texas) to monitor sap flow in three canopy layers. These gauges utilize the stem heat balance (SHB) method, whereby an insulated heater supplying a measured quantity of heat is placed around the circumference of the stem. Temperature measurements are made above and below the heater and within the heater insulation to determine heat losses to the ambient environment. The remaining heat loss T_i is accounted for by sap flow [*Van Bavel and Van Bavel*, 1990]. The sap flux gauges were shielded with aluminum foil to minimize stem thermal gradients after *Gutierrez et al.* [1994]. All gauges were wired to a Delta-T DL2 datalogger (Delta-T Devices Ltd, Cambridge, England) equipped with 60 differential channels. Data were sampled at 30 s intervals and averaged over 30 min periods. To convert sap flow to transpiration (T) at the chamber level, the measurement tree was harvested and a representative leaf area (L_A) was estimated as follows: Square paper cutouts of known area were weighed in order to develop a relationship between paper weight and area. Then, 10 leaves from each of the three canopy layers were photocopied onto paper from the same stock as the area calibration, and the cutouts were weighed to predict the area of each leaf. The leaves were oven dried for 48 hours at 70°C to determine the specific leaf area for each canopy layer. The remaining leaves from each layer were also oven dried, and L_A was estimated from the dry weight of foliage in all three layers and respective specific leaf area. In order to convert T_i to $T(=T_i\ \mathrm{LAI}/L_A)$, the chamber area index (LAI) was estimated using a LAI-2000 Plant Canopy Analyzer (LICOR Inc, Lincoln, Nebraska) which was used with one overstory measurement inside the chamber and five understory measurements taken at various locations throughout the chamber at ground level. The two outer light detectors, operating at 61°–74° and 47°–58° were excluded from the calculations so that the LAI value would not encompass area outside the chamber. The resultant LAI for the chamber was 2.83(±0.12).

Table 1. Summary of Root Density Measurements for *Quercus phellos L.*

Sample	Depth, cm	Root Density, m/m^3
1A	0–10	10,063
	10–20	1835
	20–30	571
1B	0–10	11,659
	10–20	4586
	20–30	2246

3.3. Root-Density Measurements

Root density was measured with a soil core at two locations within the chamber. The cores were separated into 10-cm layers and the roots were extracted from the soil volume by washing them through sieves (size is 2 mm). After scanning the root extracts using an HP Scanjet (11C/ADF; 600 dpi), the root length was estimated using a computer imaging software NIH Image (National Institute of Health) and root density was calculated. The root density measurements for each 10 cm layer are presented in Table 1. These results show that 90% of the root density is concentrated in the top 20 cm. While it is desirable to obtain many more root density measurements, such measurements are destructive and can alter the tree growth and physiological responses to environmental conditions, moisture content measurements, and the natural development of the tree rooting system in the chamber.

3.4. Estimation of Soil Hydraulic Properties

Saturated hydraulic conductivity was estimated from a compact constant head permeameter (Ksat, Inc., Raleigh, North Carolina) which measures the steady state flow of water through the soil horizons [*Amoozegar*, 1989]. The saturated soil water content value was set to the highest moisture content recorded following an intensive precipitation event. The effective values for the empirical parameters b and Ψ_s were calculated using the measured θ and Ψ at the nine locations in the chamber via a linear regression of the form

$$\ln(\Psi) = -b \ln\left(\frac{\theta}{\theta_s}\right) + \ln(\Psi_s) \qquad (12)$$

for each of the three layers. The optimal regression fit was obtained by combining measurements from 0 to 10 cm and 10 to 20 cm (soil + root system), with the 20 to 30 cm (soil) estimated separately. The variance around each hydraulic parameter was also estimated from the regression analysis and summarized in Table 2. Figure 2 presents the *Clapp and Hornberger* [1978] optimal regression fit using (12) to the Watermark measured Ψ and TDR measured θ for the 0–20 cm and 20–30 cm layers. Departures between the estimated values in Table 2 and the *Clapp and Hornberger* [1978] (Table 2) values is partially attributed to the preferential flow due to the large

Table 2. Soil Hydraulic Properties

Soil Hydraulic Properties	0–20 cm	20–30 cm	>30 cm
K_s, mm/d	58 (±10)	58 (±10)	200
b	2.31 (±0.1)	4.16 (±0.224)	1.34
$-\Psi_s$, mm	140.57 (±63.55)	40.56 (±15.53)	587.0
θ_s, cm^3/cm^3	0.4 (±0.01)	0.4 (±0.01)	0.4

Standard deviations in parentheses.

pores created by the root system [see, e.g., *Moore et al.*, 1986] and the artificial homogeneization (roller tilling) of the top 30 cm of the soil prior to the chamber installation. We note that large pores tend to reduce the empirical coefficient b and increase the saturated hydraulic conductivity. This trend is consistent with the data of *Clapp and Hornberger* [1978] (Table 2) where the b value for sand (large pores) is much smaller than the values for sandy clay or clay (small pores).

3.5. Comments on Spatial Statistics and Integral Length Scales of Near-Surface θ

In order to assess the statistical structure of the spatial variability of the near-surface soil moisture content, TDR moisture content measurements along two orthogonal transects were made. Such an experiment permits an assessment of the isotropy in the moisture content statistics and provides estimates of the characteristic length scales. For this purpose, a separate experiment was carried out on July 27, 1995, where a NE-SW and NW-SE transects were instrumented with 10 cm TDR rods at spatial increments of 10 cm. The same experiment was repeated on August 5, 1995, but along a N-S and E-W transect. Hence 30 TDR moisture content measurements per transect were available and are shown in Figure 3a. Table 3 shows a summary of these statistics, and Figure 3b shows the autocorrelation function $\rho(s)$ for spatial lag (s) up to 1 m. The 95% confidence limits were estimated from *Salas et al.* [1980, p. 49]. Notice in Figure 3b the rapid decay in $\rho(s)$ with significant correlation occurring only at $s = 0.1$ m. This correlation may be attributed to the overlap in TDR volume averaging at each location since the two rods forming the waveguides were spaced at 5–6 cm apart. Hence, for the purpose of this study,

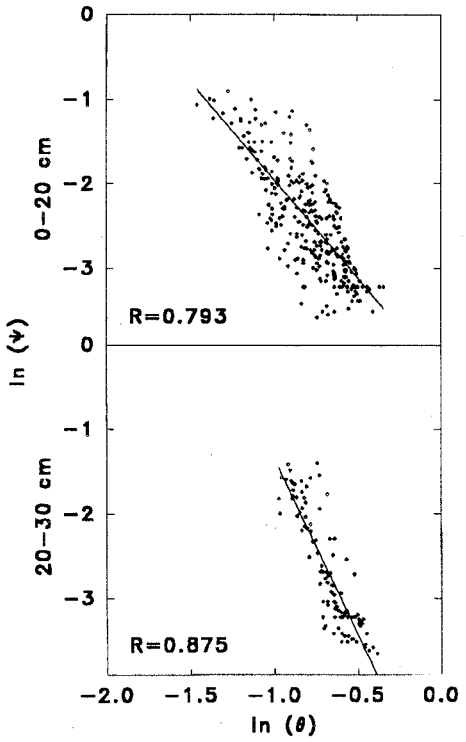

Figure 2. Determination of the soil water characteristic curve and the *Clapp and Hornberger* [1978] soil hydraulic parameters. The TDR and block resistance measurements, and the linear regression fit $\ln|\Psi| = -b \ln(\theta/\theta_s) + \ln|\Psi_s|$ are shown for the 0–20 cm and 20–30 cm layers for all seven drying cycles.

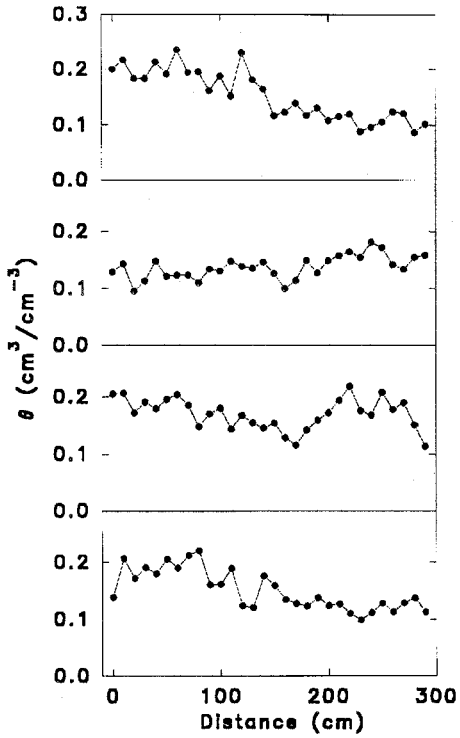

Figure 3a. Variation of soil moisture content (0–10 cm layer) along two pairs of orthogonal transects. (top) The first transect is along N-S, the second is along the E-W, the third is along the NE-SW, and (bottom) the fourth is along the NW-SE. The spacing between measurements is 10 cm.

Table 3. Summary Moisture Content Statistics Along the Two Transects

	Transect			
	N-S	E-W	NE-SW	NW-SE
n	30	30	30	30
Mean	0.15	0.14	0.17	0.15
SD	0.04	0.02	0.03	0.03
CV	0.29	0.15	0.16	0.23
Kurtosis	1.80	2.70	2.50	2.30

The sample size (n), mean, standard deviation (SD), coefficient of variation (CV), and the dimensionless fourth moment (Kurtosis) are also presented. For Gaussian distributed variables the Kurtosis is 3.0.

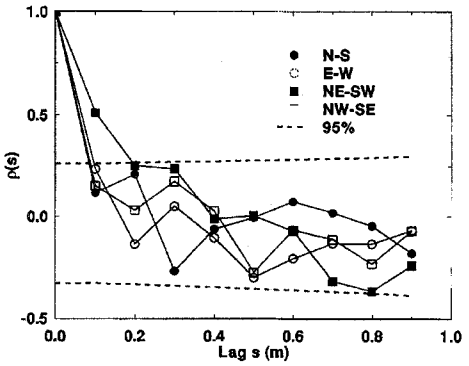

Figure 3b. Spatial moisture content covariance as a function of spatial lag (s) for the two transects.

it is reasonable to assume that the soil hydraulic properties are spatially independent within the chamber.

4. Results and Discussion

The experiment started on May 30, 1995, and data were collected every day until June 18, 1995. The mean air temperature and relative humidity in the chambers ranged from 11.5°C to 35.0°C, and 29% to 100%, respectively. During this period, eight precipitation events (cumulative = 97.2 mm) occurred resulting in seven drying cycles. We consider two drying cycles for which lateral flow into the chamber was negligible. The first cycle is 5.5 days in duration with 2 readings per day, the second cycle is 1.5 days in duration with 4 readings per day. These two drying cycles were also selected due to the availability of continuous transpiration measurements from the Dynagage system. Comparisons between TDR measured and predicted $\langle\theta\rangle$ using several root uptake and drainage approximations are presented in section 4.2.1 for each of the three layers. However, before these comparisons are discussed, the validity of the one-dimensional flow approximation must be assessed.

4.1. One-Dimensional Versus Three-Dimensional Water Transport Models

In (1) and (3), it was assumed that a one-dimensional flow well approximates the moisture content time variation. In order to assess this assumption, horizontal gradients must be compared to vertical gradients at every point in the chamber, which in practice, cannot be achieved. An alternate approach is to carry out an order of magnitude analysis and test whether the vertical gradients are, on average, much larger than the horizontal gradients. Such an order of magnitude calculation would require an estimate of the expected horizontal and vertical pressure variability, and horizontal and vertical length scales. These length and pressure scales define a characteristic horizontal (α_H) and a vertical (α_V) soil pressure gradient within the chamber. For operational purposes, the following quantities are used:

$$\alpha_H \sim \frac{\langle \Psi(z)'^2 \rangle^{1/2}}{2R}; \qquad \alpha_V \sim \frac{\langle \Psi(z+dz) \rangle - \langle \Psi(z) \rangle}{dz}. \tag{13}$$

In (13), the mean amplitudes of the horizontal soil pressure fluctuations within the chamber define a scale for horizontal pressure departure from a constant mean value. If the horizontal soil pressure variability is small within the chamber, $\alpha_H \to 0$ and horizontal soil-water distribution can be neglected relative to the vertical distribution. Hence a necessary (but not sufficient) condition for the validity of (1) is that $|(\alpha_V)/(\alpha_H)| \gg 1$. These scale arguments were directly tested by the Watermark soil pressure measurements for the top two layers and are shown in Figure 3c for both drying periods. Notice that $|(\alpha_v)/(\alpha_H)| > 10$ for the long drying cycle but was ≈ 1 at the beginning of the short drying cycle. Hence, for all practical purposes, the flow can be treated as one dimensional except for the beginning 0.5 days of the short drying cycle.

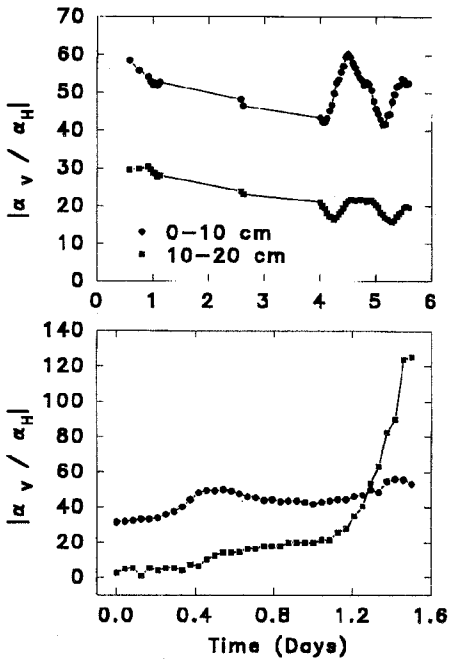

Figure 3c. Time variation of $|\alpha_v/\alpha_H|$ for the two drying cycles.

4.2. Linearized Taylor Series Expansion for the Flux

In this subsection, the moisture content mean and variance budgets are considered within the context of the linearized Taylor series expansion for the vertical flux and TDR measurements.

4.2.1. Volume Averaged Mean Moisture Content. The time evolution of $\langle\theta\rangle$ was computed from (3), (5), and (6) for each drying cycle. Four approaches to (5) and three approaches to the drainage from the z = 30 cm plane are considered.

Root Uptake: The root uptake is divided into three layers (0–10 cm, 10–20 cm, and 20–30 cm) corresponding to the measured ρ_r. The measured transpiration (T) (see Figures 4a and 4b) is multiplied by the percent root density and relative efficiency of root uptake at each of these layers. This product defines the root uptake (S) at each computational node within these three vertical layers. In discrete form, a solution to (5) can be written as

$$S_i = \frac{\rho_i W_i}{\sum_{k=1}^{k=N} \rho_k W_k} T \tag{14}$$

where i = 1, 2, $\cdots$, N is the depth node index, N is the number of vertical nodes, and S_i is the root uptake for that node, ρ_r is assumed to be constant over the intervals 0–10 cm, 10–20 cm, and 20–30 cm, and T is the measured transpiration by the sapflow gauge at time t, and W_i is a weighting function at each node. Hence (14) is an approximate scheme to distribute the transpiration loss to different soil layers based on root density and other hydraulic properties. We note that such a scheme does not consider the partitioning between dead and live roots within the ρ_r profile. However, given the small contribution to ρ_r from the 10–30 cm layers, this refinement will not be considered in (14). Four weighing schemes (hereafter referred to as root uptake models 1 to 4) are considered in (14):

Model 1 $W_i = 1$
Model 2 $W_i = \theta_i$
Model 3 $W_i = K(\theta_i)$
Model 4 $W_i = q_i$

In model 1, the roots are assumed to extract water at equal efficiencies irrespective of the moisture content state. Models 2–4 relate the efficiency of the root uptake to the available moisture content, the ability of the soil to transport water to the roots, and the actual local fluxes neighboring the roots. An analogous formulation to model 2 was proposed by *Warrick* [1974] and *Markar and Mein* [1987]. Other root water uptake models that employ electrical analogs to the root system [*Cowan*, 1965; *Herkelrath et al.*, 1977; *Campbell*, 1991] have been proposed. These models require a priori calibration for determining the corresponding resistances and will not be considered. A study by *Richards and Caldwell* [1987] suggested that a "hydraulic lift" in the root zone is responsible for the transport of water between soil layers. Given the short root zone, the concentration of root density in the top 10 cm, and the vertical variability in soil water pressure, this process is neglected relative to the soil water redistribution induced by soil pressure gradients.

Drainage (lower boundary condition): Because of the uncertainty in the lower boundary condition, we consider three approximate schemes (hereafter referred to as drainage models 1 to 3) for the bottom 30 cm layer: (1) zero drainage ($q(N) = 0$), (2) unit gradient with K(θ) defined by the hydraulic properties of the deeper soil such that

$$q(N) = 200\left(\frac{\theta}{0.4}\right)^{5.68} \tag{15}$$

and (3) unit gradient ($q(N) = K(\theta)$), where the *Clapp and Hornberger* [1978] parameters are from Table 2, and $q(N)$ is the drainage from the last layer (mm d^{-1}) determined from a separate experiment at the same site described by *Todd* [1995].

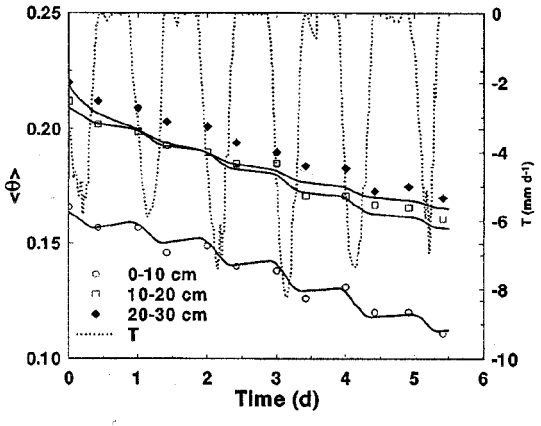

Figure 4a. Comparison between TDR measured (symbols) and predicted (solid line) $\langle\theta\rangle$ from the linearized Taylor series expansion of the vertical flux for all three layers and long drying period. The heat flux gauge measured transpiration (mm d^{-1}) is also shown (dotted line).

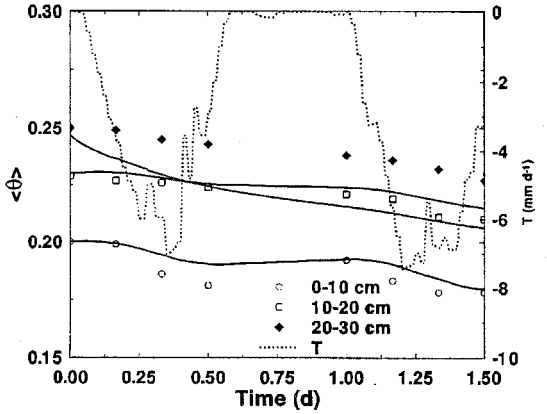

Figure 4b. Same as Figure 4a but for the short drying period.

Tables 4a, 4b, and 4c compare the predicted and measured $\langle\theta\rangle$ for all three layers, respectively for all combinations of S and $q(N)$ parameterizations. From these tables, it appears that the combination of $W_i = \theta_i$ and (15) consistently yielded good results for the longer drying period and reasonable results for the shorter period. It should be noted that the change in $\langle\theta\rangle$ for the short drying cycle is small when compared to the longer drying cycle. The comparisons between TDR measurements and predictions for this optimal combination of W_i and $q(N)$ are also shown in Figures 4a and 4b for the two drying periods, respectively and for all three layers. While the predicted 0–10 cm and 10–20 cm $\langle\theta\rangle$ are in good agreement with measured $\langle\theta\rangle$ by this approach, the 20–30 cm $\langle\theta\rangle$ are not for both drying periods. However, all the predicted $\langle\theta\rangle$ are within one standard deviation of the measured $\langle\theta'^2\rangle^{1/2}$ (not shown in Figures 4a and 4b for clarity in comparisons).

Notice in Figures 4a and 4b that the evening recharge of the top layer is significant in both TDR measurements and simulations. For both drying cycles, 20–30% of the depleted $\langle\theta\rangle$ in the top 10 cm was recharged during the evening, when $T \approx 0$, from the deeper layers. We reemphasize that the predicted recharge in Figures 4a and 4b is strictly based on soil water pressure differences and not root hydraulic lift.

4.2.2. Volume-averaged moisture content variance budget. From Appendix - A, the linearized Taylor series expansion for the variance budget reduces to

$$\frac{\partial\langle\theta'^2\rangle}{\partial t} = -\left(2\langle\theta'^2\rangle\frac{\partial F(\langle\theta\rangle)}{\partial z} + F(\langle\theta\rangle)\frac{\partial\langle\theta'^2\rangle}{\partial z} + 2\langle\theta' S'\rangle\right); \tag{16}$$

where

$$F(\langle\theta\rangle) = \frac{K_s\Psi_s b}{\theta_s^{b+3}}(b+2)\langle\theta\rangle^{b+1}\frac{\partial\langle\theta\rangle}{\partial z} + \frac{K_s}{\theta_s^{2b+3}}(2b+3)\langle\theta\rangle^{2b+2}.$$

Table 4a. Comparison Between Modeled and Measured $\langle\theta\rangle$ for the 0–10 cm Layer

Drying Cycle	Drainage Model	Root Uptake	A	B	R^2	SEE	n
1	1	1	1.09	−0.0093	0.98	0.0025	12
		2	0.97	0.0099	0.98	0.0022	12
		3	0.83	0.035	0.98	0.0023	12
		4	1.00	0.003	0.98	0.0021	12
	2	1	1.09	−0.01	0.98	0.0025	12
		2	1.00	0.005	0.98	0.0023	12
		3	0.91	0.022	0.97	0.0027	12
		4	1.32	−0.05	0.97	0.0031	12
	3	1	1.09	−0.0094	0.98	0.0022	12
		2	0.98	0.0096	0.98	0.0024	12
		3	0.84	0.033	0.97	0.0024	12
		4	1.03	−0.0005	0.98	0.0022	12
2	1	1	0.67	0.072	0.77	0.003	8
		2	0.69	0.067	0.79	0.003	8
		3	0.59	0.087	0.77	0.003	8
		4	0.67	0.072	0.77	0.003	8
	2	1	0.74	0.057	0.79	0.004	8
		2	0.70	0.065	0.79	0.003	8
		3	0.63	0.080	0.77	0.003	8
		4	1.05	−0.005	0.77	0.005	8
	3	1	0.74	0.058	0.79	0.0036	8
		2	0.69	0.067	0.79	0.0034	8
		3	0.60	0.086	0.77	0.0031	8
		4	0.70	0.065	0.77	0.0036	8

The statistics for the drying period (1, long; 2, short), the drainage model (1, 2, and 3, correspond to $q(n) = 0$, (15), and $K(\theta)$), and the root uptake weighing scheme are presented. The regression model is of the form $\langle\theta\rangle^{(\text{model})} = A\langle\theta\rangle^{(\text{TDR})} + B$. The coefficient of determination (R^2), the standard error of estimate (SEE), and the number of points used in the regression (n) are also shown.

In many field experiments, the spatial variability in θ due to root uptake is neglected (see, e.g., review by *White* [1988] and *Clothier* [1988]). Hence no a priori estimate of the relative importance of this covariance term is currently available. To assess the importance of this term relative to the other terms in (16), the following procedure was used in each drying cycle: (1) Estimate $\partial\langle\theta'^2\rangle/\partial t$ using the slopes A of the linear regression $\langle\theta'^2\rangle = At + B$, where $\langle\theta'^2\rangle$ is measured by the TDR at each of the three layers. The resulting regression fits are shown in Figure 5a. Notice in Figure 5a that the regression slope is 3 times smaller in the 20–30 cm layer versus the upper 0–20 cm layers, where the root activity is large. (2) Estimate $F(\langle\theta\rangle)$ for

Table 4b. Same as Table 4a but for the 10–20 cm Layer

Drying Cycle	Drainage Model	Root Uptake	A	B	R^2	SEE	n
1	1	1	0.96	0.068	0.98	0.00192	12
		2	1.00	−0.001	0.98	0.00198	12
		3	1.18	−0.04	0.99	0.0020	12
		4	1.17	−0.036	0.98	0.0023	12
	2	1	0.99	0.0011	0.98	0.0020	12
		2	1.04	−0.0098	0.98	0.0021	12
		3	1.28	−0.062	0.98	0.0023	12
		4	1.37	−0.080	0.97	0.0035	12
	3	1	0.96	0.0073	0.98	0.00193	12
		2	1.00	−0.0021	0.98	0.0020	12
		3	1.19	−0.043	0.99	0.0021	12
		4	1.18	−0.040	0.98	0.0023	12
2	1	1	0.89	0.025	0.95	0.0016	8
		2	0.71	0.068	0.96	0.0011	8
		3	0.90	0.023	0.95	0.0016	8
		4	0.89	0.025	0.95	0.0016	8
	2	1	0.72	0.065	0.96	0.0011	8
		2	0.75	0.058	0.96	0.0011	8
		3	0.98	0.005	0.95	0.0017	8
		4	1.32	−0.072	0.93	0.0027	8
	3	1	0.69	0.072	0.96	0.0011	8
		2	0.71	0.066	0.96	0.0011	8
		3	0.92	0.020	0.95	0.0017	8
		4	0.67	0.073	0.96	0.0012	8

Table 4c. Same as Table 4a but for the 20–30 cm Layer

Drying Cycle	Drainage Model	Root Uptake	A	B	R^2	SEE	n
1	1	1	0.448	0.122	0.99	0.0005	12
		2	0.526	0.105	0.99	0.00069	12
		3	0.501	0.111	0.98	0.0011	12
		4	0.325	0.150	0.96	0.0010	12
	2	1	0.94	0.006	0.96	0.0032	12
		2	0.98	−0.0033	0.97	0.0031	12
		3	0.90	0.015	0.96	0.0032	12
		4	0.67	0.066	0.90	0.0035	12
	3	1	0.50	0.11	0.99	0.0006	12
		2	0.57	0.095	0.99	0.0006	12
		3	0.54	0.10	0.98	0.0009	12
		4	0.36	0.142	0.97	0.0009	12
2	1	1	0.40	0.15	0.99	0.0004	8
		2	0.55	0.11	0.98	0.0007	8
		3	0.49	0.13	0.98	0.0006	8
		4	0.40	0.15	0.99	0.0004	8
	2	1	1.65	−0.17	0.92	0.0044	8
		2	1.66	−0.18	0.92	0.0044	8
		3	1.58	−0.15	0.90	0.0045	8
		4	1.29	−0.08	0.86	0.0046	8
	3	1	0.70	0.07	0.98	0.0009	8
		2	0.73	0.065	0.98	0.0009	8
		3	0.658	0.082	0.97	0.0009	8
		4	0.540	0.112	0.97	0.0008	8

all three layers using the TDR measured $\langle\theta\rangle$. (3) Estimate P_I from the linearized Taylor series expansion for the flux (see Appendix A) using

$$P_I \approx 2\langle\theta'^2\rangle \frac{\partial F(\langle\theta\rangle)}{\partial z} + F(\langle\theta\rangle)\frac{\partial\langle\theta'^2\rangle}{\partial z}.$$

Explicit finite differencing for all partial derivatives is employed. (4) Estimate $-2\langle\theta' S'\rangle$ by subtracting the estimated P_I from the regression results in step (1). Figure 5b displays the time evolution of $-2\langle\theta' S'\rangle$ along with the other two components of the variance budget ($\partial\langle\theta'^2\rangle/\partial t$, P_I) for the first drying cycle. Notice in Figure 5b that $-2\langle\theta' S'\rangle$ is comparable in magnitude to P_I in the top 10 cm of the soil. Initially, $-2\langle\theta' S'\rangle$ is positive, suggesting that for wetter conditions, the soil water root uptake is increasing the moisture content variance. However, as the drying cycle continues, $-2\langle\theta' S'\rangle$ reverses signs and becomes negative contributing to the reduction in moisture content variance. Also, as the soil moisture content is depleted, the contribution of P_I to the variance budget diminishes and $-2\langle\theta' S'\rangle$ appears to be the main contributor (2–4 times more than P_I) to the variance dissipation. This estimate is also consistent with the differences in regression slopes of Figure 5a for $\partial\langle\theta'^2\rangle/\partial t$ in the 10–20 cm and 20–30 cm layers. For the deeper layers, the dissipation of $\langle\theta'^2\rangle$ is much less rapid when compared to the 0–10 cm layer due to the minor contribution of $-2\langle\theta' S'\rangle$.

4.3. Stochastic Simulations

The linearized Taylor series expansion for the flux does not consider explicitly the horizontal variability in soil hydraulic properties as evidenced by the approximation in (6). To esti-

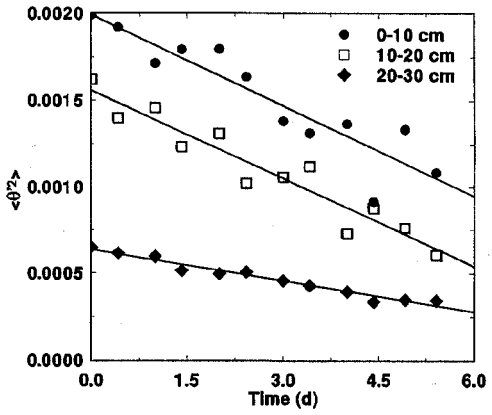

Figure 5a. TDR measured time variation of $\langle\theta'^2\rangle$ for all three layers and long drying period. The regression lines are also shown.

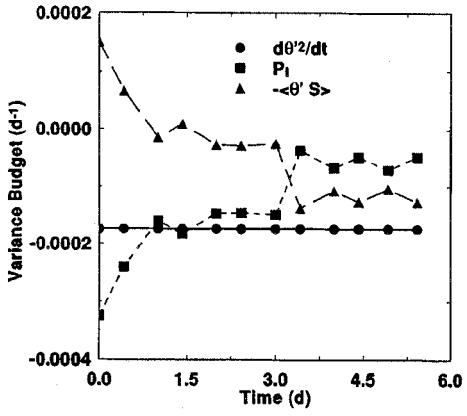

Figure 5b. The time evolution of the variance budget terms $-2\langle\theta' S'\rangle$ (estimated as a residual in (9)), P_I (estimated from (A9)), $\partial\langle\theta'^2\rangle/\partial t$ (fitted to the $\langle\theta'^2\rangle$ time TDR measurements) variance budget for the long drying period.

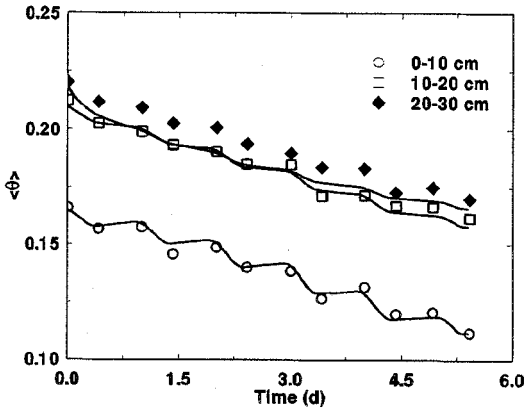

Figure 6a. Same as Figure 4a but using the stochastic simulations approach.

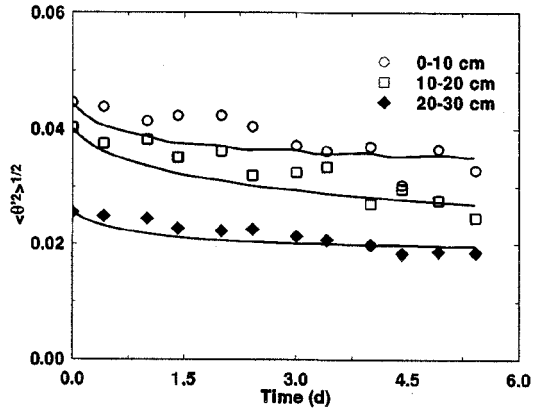

Figure 6b. Comparison between TDR measured and predicted $\langle\theta'^2\rangle^{1/2}$ for all three layers and long drying cycle.

mate how important this variability is on the measured variance, Monte Carlo simulations were carried out. Using the variance in soil hydraulic properties (see Table 2) and setting as initial conditions the measured $\langle\theta\rangle$ and $\langle\theta'^2\rangle$, 1000 simulations were used to solve (3).

In essence, this approach decomposes the chamber into a series of soil-columns, with each column having a set of soil properties and transpiring at T. For each column, (1), (4), and (5) can be solved, and the horizontally averaged moisture content for the chamber can be constructed by averaging the moisture content time series of all the columns in the chamber. On the basis of the zero integral length scale estimates of section 3.5, the columns are, to a first approximation, independent. Details of these simulations are presented in Appendix B. These simulations were performed with root uptake model 2 and drainage model 2 given the analysis in Tables 4a to 4c.

4.3.1. Ensemble mean. Figure 6a displays the ensemble predicted and TDR measured $\langle\theta\rangle$ for the long drying cycle and all three depths. Good agreement between the linearized Taylor series expansion, the Monte-Carlo simulations, and the TDR measurements is noted.

4.3.2. Ensemble variance. Figure 6b displays the ensemble predicted and measured $\langle\theta'^2\rangle^{1/2}$ for the long drying cycle. In this analysis, the following were assumed:

1. The root uptake and moisture content interaction (P_{II}) is indirectly accounted for by root uptake model 2. In this model, the sink is a linear function of moisture content and transpiration.
2. The transpiration is assumed to be constant in space throughout the chamber.
3. The distribution of the soil hydraulic parameters is Gaussian, isotropic, with zero correlation length scales within the 3.1 m chamber diameter. It should be noted that several studies demonstrated that K_s is lognormally distributed [*Bigger and Nielsen*, 1976]. However, given the limited variability in K_s, the small chamber size, the limited number of K_s measurements, and the microsite variability, we assumed that K_s is Gaussian with a coefficient of variation set to 0.15.

Despite these approximations, good agreement between simulated and measured $\langle\theta'^2\rangle^{1/2}$ is noted and is well within the standard error of estimate by *Topp et al.* [1980] calibration curve ($\approx$0.01 cm^3 cm^{-3}). To better illustrate the variation in $\langle\theta'^2\rangle^{1/2}$ relative to $\langle\theta\rangle$, Figure 6c displays the measured and predicted coefficient of variation (CV = $\langle\theta'^2\rangle^{1/2}/\langle\theta\rangle$), for all three layers. Interestingly, the measured and predicted CV are very comparable to the CV reported from a wide range of field experiments [see *White*, 1988; Table 3; *Warrick and Nielsen*, 1980], though care must be taken in comparing CV from different experiments since sample size and volume can dramatically alter the frequency distribution and the magnitude of CV as discussed by *Sisson and Wierenga* [1981].

5. Conclusions

This study considered the time-space variation of soil moisture in the root zone of willow oak saplings within a 3.1-m chamber. Such a scale is between the laboratory and the field. It was shown from an order of magnitude analysis and detailed measurement of soil water pressure that a one-dimensional flow is a valid approximation within this chamber. The one-dimensional flow approximation was used to derive prognostic equations for the time variation of the spatial mean and variance moisture content budgets. Comparisons with direct TDR measurements along a three dimensional grid was performed for two drying cycles: The following can be concluded:

1. While the coefficient of variation in the spatial statistics of soil moisture content are comparable to much larger field-

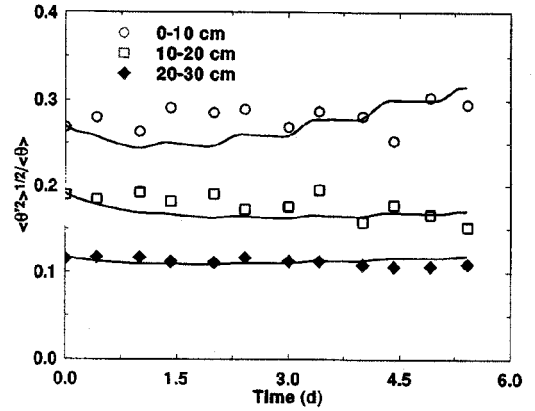

Figure 6c. Same as Figure 6b but for the coefficient of variation (CV).

scale experiments [e.g., *Nielsen et al.*, 1973; *Mulla*, 1988; *Buchter et al.*, 1991], the proposed linearized Taylor series expansion for the vertical flux resulted in predictions that agree well with the TDR measurements at least for the mean moisture content state. Our study suggests that when root water uptake is a significant term in the continuity equation, a first-order Taylor series expansion for the water flux is sufficient to the accurate description of the mean moisture content.

2. The moisture content variance budget was derived and two dynamical processes were shown to be responsible for the time variation of the moisture content spatial variance. These processes involve the spatial interaction between the moisture content and the vertical flux gradient perturbations (P_{I}), and the moisture content and the root uptake perturbations (P_{II}). On the basis of proposed linearized Taylor series expansion for the flux and the measured time variation of the spatial moisture content variance, P_{II} was estimated and found to be 2–3 times larger than P_{I} in the primary root zone and for dry soil conditions. For wetter soil conditions, P_{II} was a moisture content variance production term; however, in magnitude, it appeared to be smaller than P_{I}. Hence this study demonstrates that root water uptake variability can be an important mechanism in the time evolution of the moisture content variance field.

3. An approximate scheme that relates root water uptake, soil moisture content, and transpiration was proposed and tested with TDR measurements. This scheme reproduced the time variation of the measured spatial mean and variance moisture content in the top 20 cm layer. A key advantage to the proposed scheme is its suitability for Monte Carlo solutions to the continuity equation given the time variation of the transpiration.

4. The diurnal variation of transpiration and root water uptake resulted in a 20–30% evening recharge for the top 10 cm from deeper layers. This large recharge in the top 10-cm layer was captured by both simulations and TDR measurements. Matric potential gradients where sufficient to explain this recharge without the need to invoke a root hydraulic lift assumption. Our study showed that accounting for the diurnal trends in transpiration is necessary to the accurate description of near-surface moisture content, which is central to the partitioning of net radiation into sensible, latent, and soil heat fluxes close to the land-atmosphere interface.

Appendix A: Approximate Analytic Equations for the Mean and Variance Moisture Content

In this appendix, the assumptions and consequences of the linearlized Taylor series expansion for the vertical flux, used to derive prognostic equations for the budgets of moisture content mean and variance, are discussed.

A.1. Mean Moisture Content Equation

From (3), the time evolution of $\langle\theta\rangle$ is rewritten as

$$\frac{\partial\langle\theta\rangle}{\partial t} = -\left(\frac{\partial\langle q\rangle}{\partial z} + \langle S\rangle\right) \tag{A1}$$

In order to evaluate $\langle q\rangle$, consider a simplified one-dimensional Taylor series expansion of q around $\langle\theta\rangle$, which is given by

$$q(\theta) = q(\langle\theta\rangle) + \left.\frac{\partial q}{\partial\theta}\right|_{\langle\theta\rangle}(\theta - \langle\theta\rangle) + \frac{1}{2!}\left.\frac{\partial^2 q}{\partial\theta^2}\right|_{\langle\theta\rangle}(\theta - \langle\theta\rangle)^2 + \frac{1}{3!}\left.\frac{\partial^3 q}{\partial\theta^3}\right|_{\langle\theta\rangle}(\theta - \langle\theta\rangle)^3 + \cdots$$

By truncating the expansion at the second term, q simplifies to

$$q(\theta) \approx q(\langle\theta\rangle) + \left.\frac{\partial q}{\partial\theta}\right|_{\langle\theta\rangle}(\theta - \langle\theta\rangle) \tag{A2}$$

which, upon volume averaging, reduces to

$$\langle q(\theta)\rangle \approx q(\langle\theta\rangle) \tag{A3}$$

where $q(\langle\theta\rangle)$ is computed from (4) and is given by

$$q(\langle\theta\rangle) = \frac{K_s\Psi_s b}{\theta_s^{b+3}}(\langle\theta\rangle)^{b+2}\frac{\partial\langle\theta\rangle}{\partial z} + K_s\left(\frac{\langle\theta\rangle}{\theta_s}\right)^{2b+3} \tag{A4}$$

which is the approximation in (6).

A.2. Moisture Content Variance Equation

By subtracting (3) from (1) and multiplying the resultant equation by $2(\theta - \langle\theta\rangle)$,

$$2(\theta - \langle\theta\rangle)\frac{\partial(\theta - \langle\theta\rangle)}{\partial t} = -\Big(2(\theta - \langle\theta\rangle)\frac{\partial}{\partial z}[q(\theta) - q(\langle\theta\rangle)] + 2(\theta - \langle\theta\rangle)(S - \langle S\rangle)\Big)$$

which upon volume averaging, gives

$$\frac{\partial\langle\theta'^2\rangle}{\partial t} = -(P_I + P_{II})$$

$$P_I = 2\left\langle\theta'\frac{\partial}{\partial z}(q(\theta) - q(\langle\theta\rangle))\right\rangle \tag{A5}$$

$$P_{II} = 2\langle\theta' S'\rangle$$

In order to evaluate P_I, replace (A2) in (A5) so that

$$P_I = 2\left\langle\theta'\frac{\partial}{\partial z}\left[\frac{\partial q}{\partial\theta}(\theta')\right]\right\rangle \tag{A6}$$

Using (7) and (8), the derivative

$$\frac{\partial q}{\partial\theta} = \frac{K_s\Psi_s b}{\theta_s^{b+3}}(b+2)\langle\theta\rangle^{b+1}\frac{\partial\langle\theta\rangle}{\partial z} + \frac{K_s}{\theta_s^{2b+3}}(2b+3)\langle\theta\rangle^{2b+2} = F(\langle\theta\rangle). \tag{A7}$$

Hence, by replacing (A7) in (A6), and noting that

$$\theta'\frac{\partial}{\partial z}(F(\langle\theta\rangle)\theta') = \theta'^2\frac{\partial F(\langle\theta\rangle)}{\partial z} + \theta'\frac{\partial\theta'}{\partial z}F(\langle\theta\rangle)$$

$$= \theta'^2\frac{\partial F(\langle\theta\rangle)}{\partial z} + \frac{1}{2}F(\langle\theta\rangle)\frac{\partial\theta'^2}{\partial z} \tag{A8}$$

P_{I} simplifies to

$$P_I = 2\langle\theta'^2\rangle\frac{\partial F(\langle\theta\rangle)}{\partial z} + F(\langle\theta\rangle)\frac{\partial\langle\theta'^2\rangle}{\partial z} \tag{A9}$$

and the variance budget equation becomes

$$\frac{\partial\langle\theta'^2\rangle}{\partial t} = -\left(2\langle\theta'^2\rangle\frac{\partial F(\langle\theta\rangle)}{\partial z} + F(\langle\theta\rangle)\frac{\partial\langle\theta'^2\rangle}{\partial z} + 2\langle\theta' S'\rangle\right)$$

where $F(\langle\theta\rangle)$ is given by (A7).

Appendix B: Numerical Simulation Details

In this appendix, details regarding the stochastic simulations algorithm, and boundary conditions are provided.

In the stochastic simulation approach, the parameters K_s, Ψ_s, θ_s, b are random variables in the lateral direction within the chamber. Each of these four parameters are decomposed into ensemble means ($\langle K_s \rangle$, $\langle \Psi_s \rangle$, $\langle \theta_s \rangle$, $\langle b \rangle$) and Gaussian perturbations K_s', Ψ_s', θ_s', b' such that $\langle K_s' \rangle = \langle \Psi_s' \rangle = \langle \theta_s' \rangle = \langle b' \rangle = \langle T' \rangle = 0$. We chose a Gaussian perturbation since the chamber scale (≈3.1 m) is very small when compared to the field scale (≈100 m), and thus existing variability cannot be organized and is attributed to high wavenumber random disturbances that result in Gaussian soil hydraulic properties in space in accord with the central limit theorem [*Gardiner*, 1990; pp. 37–39]. Hence (1), (4), and (5) can be solved for each combination of K_s, Ψ_s, θ_s, b, and T random samples, and the solution to (2) can be determined by ensemble averaging a large population of these runs.

B.1. Random Number Generation

It was assumed that the soil properties K_s, Ψ_s, θ_s, b can be decomposed into a mean $\langle K_s \rangle$, $\langle \Psi_s \rangle$, $\langle \theta_s \rangle$, $\langle b \rangle$ and a perturbation component K_s', Ψ_s', θ_s', b' for each soil layer, and that the perturbations are Gaussian in accord with small-scale variability and the central limit theorem. In the stochastic simulations, the parameters K_s, Ψ_s, θ_s, and b are first stored in a vector U_i (i = 1, 2, 3, and 4), respectively. The vector U_i can be decomposed into a mean $\langle U_i \rangle$ and a perturbation about the mean U_i'. As discussed in the experimental setup, $\langle U_i \rangle$ and $\langle U_i'^2 \rangle)^{1/2}$ are measured or estimated for the three layers (0–10 cm, 10–20 cm, and 20–30 cm) using the measured $\Psi - \theta$ in Figure 2. For each simulation, a zero-mean unit variance Gaussian sequence is generated using the Gaussian random number generation routine by *Press et al.* [1991, p. 145]. From this sequence, four values are sampled and stored in vector G_j (j = 1, 2, ⋯, 4). The parameters of U_i are simply constructed from the sum $\langle U_i \rangle + \langle U_i'^2 \rangle^{1/2} G_i$ for all four soil hydraulic variables.

B.2. Numerical Simulations

The root zone is discretized by 30 nodes (dz = 1 cm), and at each node, the vector U_i, is constructed as discussed above. Recall that $\langle U_i \rangle$, $\langle U_i'^2 \rangle^{1/2}$ are constant for the first 20 nodes, and the last 10 nodes, but the actual soil hydraulic properties are not. The schemes discussed below are also used in the numerical solution of (3).

B.2.1. Depth integration. Using the soil hydraulic properties and an initial soil-moisture profile, the hydraulic conductivity $K(\theta)$ and the total matric potential $H(\theta)$ are computed at each node using (7) and (8). The flux between nodes is computed using (4), where $K(\theta)$ is the average hydraulic conductivity between two consecutive nodes in (4).

B.2.2. Root-uptake (upper boundary condition). The root water uptake is divided into three layers (0–10 cm, 10–20 cm, and 20–30 cm) corresponding to the measured root density. The measured transpiration (T) is multiplied by the percent roots and relative efficiency of root uptake in each of these layers as in (14).

B.2.3. Drainage (lower boundary condition). The flux at the last node $q(N)$ must be specified in this numerical scheme, and three schemes were tested: $q(N) = 0$; $q(N) = K(\theta)$; and $q(N) = 200(\theta/0.4)^{5.68}$.

B.2.4. Time Integration. Since q and S are determined for each node, (1) can be integrated in time using a $dt = 0.001$ days. An explicit finite difference approximation is used, and at each computational node,

$$\theta_i^{(t+dt)} = \theta_i^t + dt\left(\frac{q_{i+1}^t - q_i^t}{dz}\right) + dt\ S_i^t \qquad \text{(B1)}$$

where the superscript indicates the time domain and the subscripts indicates the depth node.

B.3. Ensemble Statistics

In the stochastic simulations, the numerical solution was applied to 1000 runs using the perturbation scheme described in section B.1. In order to compare with the TDR measurements, we averaged the nodes between 0–10 cm (layer 1), 10–20 cm (layer 2), and 20–30 cm (layer 3). Thus, at each time instant, 1000 volume-averaged moisture content values were available for each of the three layers. These 1000 values were first averaged and the standard deviation about this average was computed at each dt time increment. Thus the solutions to (3) and (9) are generated by plotting the ensemble mean and standard deviation in time as shown in Figures 6a and 6b, respectively.

Acknowledgments. We would like to thank David Tremmel at the Duke University Phytotron for his assistance in finding root density with the computer imaging systems (National Institute of Health imaging analysis program), Fred Mowry for setting up the BVOC chamber site at the Duke Forest and measuring the leaf area, Brent Ewers for assisting in the moisture content measurements during the transect experiment, John Sigmon for his support through out this project, Mike Goltz for his assistance with the automated logging and operation of the Watermark blocks, and Charles Todd for his assistance in producing Figure 1. This project was funded by the Environmental Protection Agency (EPA) under the cooperative agreement 91-0074-94 (CR817766).

References

Ammozegar, A., A compact constant head permeameter for measuring saturated hydraulic conductivity of the vadose zone, *Soil Sci. Soc. Am. J.*, *5*, 1356–1361, 1989.

Armstrong, C. F., J. T. Ligon, and S. J. Thomson, Calibration of Watermark model 200 soil moisture sensor, paper presented at Summer Meeting, Am. Soc. of Agri. Eng., Mich. State Univ., East Lansing, June 23–26, 1985.

Bigger, J. W., and D. R. Nielsen, Spatial variability of the leaching characteristics of a field soil, *Water Resour. Res.*, *12*, 78–84, 1976.

Brooks, R. H., and A. T. Corey, Hydraulic properties of porous media, *Hydrol. Pap. 3*, Colo. State Univ., Fort Collins, 1964.

Buchter, B., P. O. Aina, A. S. Azari, and D. R. Nielsen, Soil spatial variability along transects, *Soil Technol.*, *4*, 297–314, 1991.

Campbell, G. S., A simple method for determining unsaturated conductivity from moisture retention data, *Soil Sci.*, *117*, 311–314, 1974.

Campbell, G. S., Simulation of water uptake by plant roots, in *Modeling Plant and Soil Systems, Agron. Monogr. Ser.*, vol. 31, edited by J. Hanks and J. T. Ritchie, pp. 273–285, Am. Soc. of Agron., Madison, Wisc., 1991.

Cassel, D. K., R. G. Kachanoski, and G. C. Topp, Practical consideration for using a TDR cable tester, *Soil Technol.*, *7*, 113–126, 1994.

Clapp, R. B., and G. M. Hornberger, Empirical equations for some soil hydraulic properties, *Water Resour. Res.*, *14*, 601–604, 1978.

Clapp, R. B., G. M. Hornberger, and B. J. Cosby, Estimating spatial variability in soil using a simplified dynamic model, *Water Resour. Res.*, *19*, 739–745, 1983.

Clothier, B. E., Measurement of soil physical properties in the field: Commentary, in *Flow and Transport in the Natural Environment: Advances and Applications*, edited by W. L. Steffen and O. T. Denmead, pp. 86–94, Springer-Verlag, New York, 1988.

Cowan, I. R., Transport of water in the soil-plant-atmosphere system, *J. Appl. Ecol.*, *2*, 221–239, 1965.

Dasberg, S., and J. W. Hopmans, Time domain reflectometry calibration for uniformily and nonuniformily wetted sandy and clayey loam soils, *Soil Sci. Soc. Am. J.*, *56*, 1341–1345, 1992.

Gardiner, C. W., *Handbook of Stochastic Methods*, 2nd ed., 442 pp., Springer-Verlag, New York, 1990.

Gardner, C. M. K., J. P. Bell, J. D. Cooper, T. J. Dean, N. Gardner, and M. G. Hodnett, Soil water content, in *Soil Analysis: Physical Methods*, edited by K. A. Smith and C. E. Mullins, pp. 1–74, Marcel Dekker, New York, 1990.

Gutierrez, M. V., R. A. Harrington, F. C. Meinzer, and J. C. Fownes, The effect of environmentally induced stem temperature gradients on transpiration estimates from the heat balance method in two tropical woody species, *Tree Phys.*, *14*, 179–190, 1994.

Herkelrath, W. N., E. E. Miller, and W. R. Gardner, Water uptake by plants, II, The root contact model, *Soil Sci. Soc. Am. J.*, *41*, 1039–1043, 1977.

Herkelrath, W. N., S. P. Hamburg, and F. Murphy, Automatic, real-time monitoring of soil moisture in a remote field area with time domain reflectometry, *Water Resour. Res.*, *27*, 857–864, 1991.

Jury, W. A., W. R. Gardner, and W. H. Gardner, *Soil Physics*, 5th ed., 328 pp., John Wiley, New York, 1991.

Katul, G. G., O. Wendroth, M. B. Parlange, C. Puente, M. Folegatti, and D. R. Nielsen, Estimation of in situ hydraulic conductivity function from nonlinear filtering theory, *Water Resour. Res.*, *29*, 1063–1070, 1993.

Macfall, J. S., G. A. Johnson, and P. J. Kramer, Observation of a water-depletion region surrounding loblolly pine roots by magnetic resonance imaging, *Proc. Natl. Acad. Sci.*, *87*, 1203–1207, 1990.

Malicki, M. A., and W. M. Skierucha, A manually controlled TDR soil moisture meter operating with a 300 ps rise-time needle pulse, *Irrig. Sci.*, *10*, 153–163, 1989.

Markar, M. S., and R. G. Mein, Modeling of evapotranspiration from homogeneous soils, *Water Resour. Res.*, *23*, 2001–2007, 1987.

Moore, I. D., G. J. Burch, and P. J. Wallbrink, Preferential flow and hydraulic conductivity of forest soils, *Soil Sci. Soc. Am. J.*, *50*, 876–881, 1986.

Mulla, D. J., Estimating spatial patterns in water content, matric suction, and hydraulic conductivity, *Soil Sci. Soc. Am. J.*, *52*, 1547–1553, 1988.

Nielsen, D. R., J. W. Bigger, and K. T. Erth, Spatial variability of field measured soil water properties, *Hilgardia*, *42*, 215–259, 1973.

Parlange, M. B., G. G. Katul, M. V. Folegatti, and D. R. Nielsen, Evaporation and the field scale soil water diffusivity function, *Water Resour. Res.*, *29*, 1279–1286, 1993.

Press, W. H., W. T. Vetterling, S. A. Teukolsky, and B. P. Flannery, *Numerical Recipes in Fortran: The Art of Scientific Computing*, 2nd ed., 963 pp., Cambridge Univ. Press, New York, 1992.

Richards, J. H., and M. M. Caldwell, Hydraulic lift: Substantial nocturnal water transport between soil layers by Artemisia tridentata roots, *Oecologia*, *73*, 486–489, 1987.

Roth, C. H., M. A. Malicki, and R. Plagge, Empirical evaluation of the relationship between soil dielectric constant and volumetric water content as the basis for calibrating soil moisture measurements by TDR, *Soil Sci.*, *43*, 1–13, 1992.

Salas, J. D., J. W. Delleur, V. Yevjevich, and W. L. Lane, *Applied Modeling of Hydrologic Time Series*, 484 pp., Water Resources Publ., Littleton, Colo., 1980.

Sisson, J. B., and P. J. Wierenga, Spatial variability of steady-state infiltration as a stochastic process, *Soil Sci. Soc. Am. J.*, *45*, 699–704, 1981.

Todd, P. H., Use of a local mass balance method to determine the effects of soil water content on canopy conductance and to estimate forest stand evapotranspiration in a natural forest and in growth chambers, M.S. thesis, 87 pp., Sch. of the Environ., Duke Univ., Durham, N. C., 1995.

Topp, G. C., and J. L. Davis, Measurement of soil water content using time domain reflectometry (TDR): A field evaluation, *Soil Sci. Soc. Am. J.*, *49*, 19–24, 1985.

Topp, G. C., J. L. Davis, and A. P. Annan, Electromagnetic determination of soil water content: Measurements in coaxial transmission lines, *Water Resour. Res.*, *16*, 574–582, 1980.

Van Bavel, M. G., and C. H. M. Van Bavel, *Dynagage Installation and Operation Manual*, Dynamax, Inc., Houston, Tex., 1990.

Warrick, A. W., Solution of the one-dimensional linear moisture flow equation with water extraction, *Soil Sci. Soc. Am.*, *38*, 573–576, 1974.

Warrick, A. W., and D. R. Nielsen, Spatial variability of soil physical properties in the field, in *Applications of Soil Physics*, pp. 319–344, Academic, San Diego, Calif., 1980.

Wendroth, O., G. G. Katul, M. B. Parlange, C. E. Puente, and D. R. Nielsen, A nonlinear filtering approach for determining hydraulic conductivity functions in field soils, *Soil Sci.*, *156*, 293–301, 1993.

White, I., Measurement of soil physical properties in the field, in *Flow and Transport in the Natural Environment: Advances and Applications*, edited by W. L. Steffen and O. T. Denmead, pp. 59–85, Springer-Verlag, New York, 1988.

Z. J. Kabala, Civil and Environmental Engineering, Duke University, Durham, NC 27708.

G. Katul, R. Oren, D. Pataki, and P. Todd, School of the Environment, Duke University, Durham, NC 27708-0328. (e-mail: gabrielk@env.duke.edu)

(Received March 29, 1996; revised December 20, 1996; accepted December 23, 1996.)